Proceedings of the PHOTON-2017 Conference, Geneva, Switzerland, 22 – 26 May 2017, edited by David d'Enterria, Albert de Roeck and Michelangelo Mangano, CERN Proceedings, Vol. 1/2018, CERN-Proceedings-2018-001 (CERN, Geneva, 2018)

Proton tomography by Deep Virtual Compton Scattering

M. Guidal
Institut de Physique Nucléaire d'Orsay, CNRS-IN2P3, Université Paris-Sud, Université Paris-Saclay, 91406 Orsay, France.

Abstract
We present some recent developments in the field of Generalized Parton Distribution and Deep Virtual Compton Scattering, namely the first extraction of the quark momentum-dependent proton charge radius from data.

Keywords
nucleon structure, Compton scattering, Parton Distributions

These past 20 years, Deep Virtual Compton Scattering (DVCS) has proven to be a very advantageous and effective process to probe the internal quark and gluon structure of the nucleon. DVCS consists in the high-energy exclusive lepto-production of a real photon on a hadronic target, i.e. the $\ell N \to \ell N \gamma$ reaction for a target nucleon N. Beam energies at the level of the GeV and higher are in order, so as to probe distances of the order of the fermi and lower. By virtue of a QCD factorization theorem, the DVCS process allows one to access the structure functions of the nucleon called the Generalized Parton Distributions (GPDs). These functions, currently largely unknown, contain, inter alia, informations on the correlation between the spatial and momentum distributions of quarks (and gluons) inside the nucleon, on their angular momentum contribution to the spin of the nucleon, on the pressure distributions inside the nucleon, etc. We refer the reader to Refs. [1–4] for the original articles on GPDs and to Refs. [5–10] for reviews of the domain.

We present here some recent developments in the field. We show a first quasi-model-independent measurement of the proton charge radius as a function of the quarks' momentum fraction. This is often refered to as proton tomography.

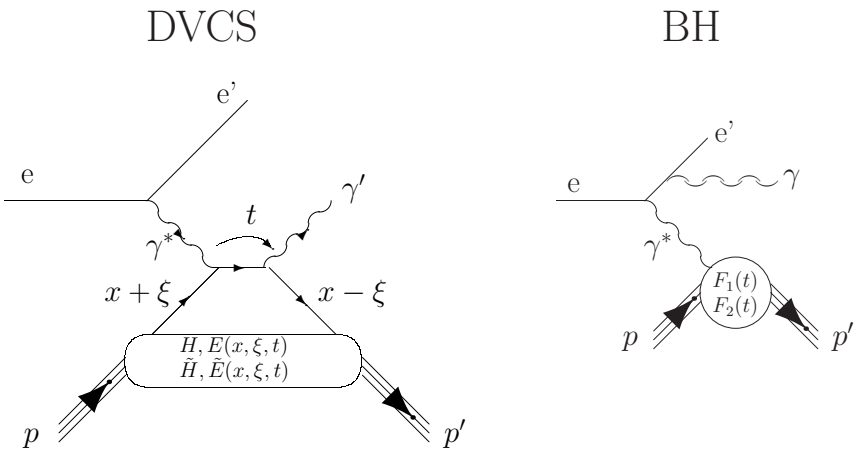

Fig. 1: Left: the DVCS process on the proton. Right: the BH process.

In the QCD leading-twist framework, in which this work takes place, there are four quark helicity-conserving GPDs, H, E, $\tilde{H}$ and $\tilde{E}$ contributing to the DVCS process (Fig. 1-left). They reflect the four independent helicity-spin transitions between the initial and final quark-nucleon systems. The dominant GPD H represents for instance the contribution of unpolarized quarks in an unpolarized nucleon.

https://doi.org/10.23727/CERN-Proceedings-2018-001.183

In the framework where QCD evolution effects are neglected, the GPDs are functions of three variables: x, ξ and t. The quantity $x+\xi$ ($x-\xi$) represents the longitudinal momentum fraction of the initial (final) quark w.r.t. the average nucleon momentum, and the variable t is the squared momentum transfer to the nucleon. This latter variable t is actually the conjugate variable of the localization of the quark in the transverse position space (impact parameter $b_\perp$), in a frame where the nucleon goes to the speed of light in a given direction [11–13]. Thus, an intuitive interpretation of GPDs is that they describe the probability amplitude of hitting a quark in the nucleon with longitudinal momentum fraction $x+\xi$ and putting it back with a different longitudinal momentum fraction $x-\xi$ at a given transverse distance $b_\perp$ in the nucleon, relative to the transverse center of mass.

Extracting the GPDs from DVCS data is a very challenging problem because:

- The four GPDs need to be disentangled. The way to do so is to measure a series of observables for the $\ell N \to \ell N\gamma$ reaction, such as unpolarized cross sections, single or double beam and/or target spin asymmetries, charge asymmmetries,... Each observable is indeed in general dominantly sensitive to a given GPD (or a specific combination of GPDs).
- GPDs appear in the DVCS amplitude in the form of integrals over x. This is due to the loop in the DVCS diagram of Fig. 1-left, which generates convolution terms such as:

$$\int_{-1}^{+1} dx \frac{GPD(x,\xi,t)}{x-\xi+i\epsilon} + ..., \tag{1}$$

  where the denominator arises from the quark propagator. Thus, only ξ and t are experimentally accessible: ξ is related to x_B, the standard Bjorken variable of Deep Inelastic Scattering, via $\xi = \frac{x_B}{2-x_B}$ and can thus be measured by detecting the scattered lepton kinematics; t is measured by detecting the recoil nucleon or the final photon.
- As a consequence of this convolution, by virtue of the residue theorem, the maximum informations that can be extracted from the experimental data at a given (ξ,t) point are quantities of the form $H(\pm\xi,\xi,t)$ when measuring an observable sensitive to the imaginary part of the DVCS amplitude, and $\int_{-1}^{+1} dx \frac{H(\mp x,\xi,t)}{x\pm\xi}$ when measuring an observable sensitive to the real part of the DVCS amplitude. In this work, we call these (real) quantities Compton Form Factors (CFFs). Since there are 4 GPDs, there are 8 CFFs.
- Another concern is that the DVCS process is not the only one contributing to the $\ell N \to \ell N\gamma$ reaction. There is also the Bethe-Heitler (BH) process in which the final state photon is radiated by the incoming or scattered lepton (see Fig. 1-right) and not by the nucleon itself like in DVCS. The BH contribution, which is quite precisely calculable, shall thus be taken into account, at the amplitude level, when extracting GPDs from experiment.

Extracting GPD information from DVCS data involves thus specialized and dedicated algorithms to adress all these issues. Several techniques have been proposed and developped these past years [10, 14–25] to extract the CFFs from different observables, with more or less model-dependency. In these short proceedings, we focus here on the fitting approach pioneered in Ref. [14] which consists in taking, at a fixed (ξ, t) kinematics, the 8 CFFs as free parameters, varying them in a systematic way in a conservatively bounded 8-fold hyperspace and, knowing the well-established BH and DVCS leading-twist amplitudes, finding the 8-CFF set which minimizes the difference between the theoretical calculation and the data. With this technique, the particular CFF $H_{Im}(\xi,t) \equiv H^q(\xi,\xi,t) - H^q(-\xi,\xi,t)$ could be extracted from several sets of polarized and unpolarized DVCS observables on the proton from the CLAS and Hall A Jefferson Lab experiments [26–29]. Fig. 2 shows such extraction of H_{Im} for several (ξ, t) bins, at different Q^2 values, where Q^2 is the squared electron momentum transfer (we recall that, in the framework in which this work is done, CFFs don't depend on Q^2) .

Although error bars, which are systematic in nature, are rather large, one can rather clearly distinguish the general behavior where there is an increase of the t-slope and of the amplitude as $t \to 0$ of H_{Im}

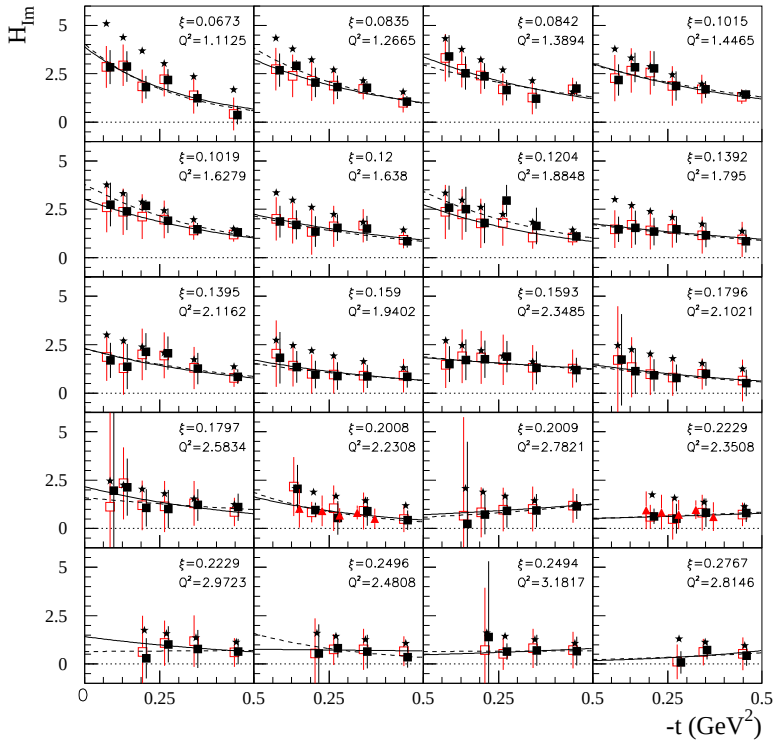

Fig. 2: The H_{Im} CFF as a function of t for 20 CLAS (ξ, Q^2) bins. The meaning of the different symbols and the precise definition of H_{Im} can be found in Ref. [25], where the figure is taken from.

as ξ decreases. Qualitatively, this reflects respectively the increase of the transverse size of the proton (since t is the conjugate variable of $b_\perp$) and of the quarks' density as smaller and smaller longitudinal quark momentum fractions are probed. In order to be quantitative and truely connect H_{Im} to a charge proton radius, a specific procedure, detailed in Ref. [25], has to be applied. It involves:

- An extrapolation of H_{Im} to $\xi = 0$, i.e. $H(\pm\xi, \xi, t)$ to $H(\pm\xi, 0, t)$,
- The connection of the singlet (quark + antiquark) to the non-singlet (quark - antiquark) contribution to which the proton radius is related. This step and the previous one carry some model-dependency, which is ultimately translated into an error bar (which is in general much lower than the uncerttainty associated to the H_{Im} fitting extraction from the data)
- A Fourier transform to shift from the momentum space variable t to the impact parameter space variable $b_\perp$. This latter step can be done analytically if a simple parametrization of H_{Im} is used as in Ref. [25].

The resulting x-momentum-dependence of the proton transverse charge radius is displayed in Fig. 3. The upper plot of Fig. 4 shows a 3-dimensional representation of the fit of Fig. 3. The bottom plot is an artistic view of the tomographic quark content of the proton, with the charge radius and the density of the quarks increasing as smaller and smaller quark momentum fractions are probed.

In summary, ithese proceedings, we have given a very brief overview of one important outcome of the GPD physics, namely the extraction the x-dependence of the proton charged radius, for the first time from DVCS data. Several new DVCS experiments are planned with the JLab upgrade at 12 GeV

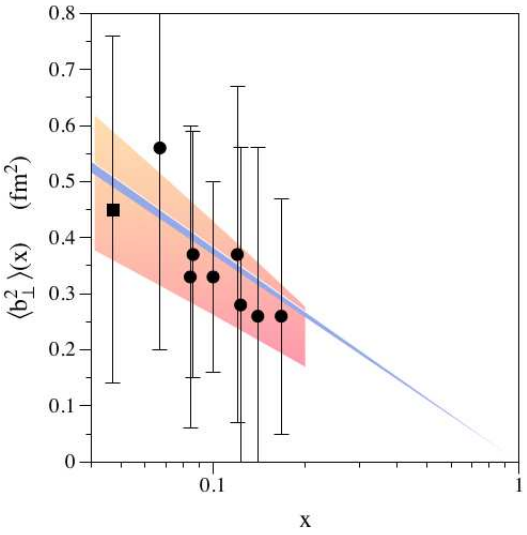

Fig. 3: x-dependence of the proton charge radius. The definition of the error bars and of the bands can be found in Ref. [25].

in the short future, which should point to important new advances coming down in the field of nucleon structure.

References

[1] X. Ji, Phys.Rev.Lett. **78**, 610 (1997).
[2] D. Mueller, D. Robaschik, B. Geyer, F. M. Dittes and J. Horejsi, Fortsch. Phys. **42**, 101 (1994).
[3] A.V. Radyushkin, Phys.Lett.B **380**, 417 (1996).
[4] X. Ji, Phys.Rev.D **55**, 7114 (1997).
[5] K. Goeke, M.V. Polyakov and M. Vanderhaeghen, Prog. Part. Nucl. Phys. **47**, 401 (2001).
[6] M. Diehl, Phys. Rept. **388**, 41 (2003).
[7] A.V. Belitsky and A. Radyushkin, Phys. Rept. **418**, 1 (2005).
[8] S. Boffi and B. Pasquini, Riv. Nuovo Cim. **30**, 387 (2007).
[9] M. Guidal, H. Moutarde and M. Vanderhaeghen, Rept. Prog. Phys. **76**, 066202 (2013).
[10] K. Kumericki, S. Liuti and H. Moutarde, Eur. Phys. J. A **52**, no. 6, 157 (2016).
[11] M. Burkardt, Phys. Rev. D **62**, 071503 (2000).
[12] J.P. Ralston and B. Pire, Phys. Rev. D **66**, 111501 (2002).
[13] M. Diehl, Eur. Phys. J. C **25**, 223 (2002); [Erratum-ibid. C **31**, 277 (2003)].
[14] M. Guidal, Eur. Phys. J. A **37**, 319 (2008). [Erratum-ibid. A **40**, 119 (2009)]
[15] K.Kumericki and D. Müller, Nucl. Phys. B **841**, 1 (2010).
[16] K. Kumericki, D. Müller and M. Murray, Nuovo Cim. C **036** (2013) no.05, 159
[17] K. Kumericki, D. Müller and M. Murray, Phys. Part. Nucl. **45** (2014) no.4, 723
[18] H. Moutarde, Phys. Rev. D **79**, 094021 (2009).
[19] M. Guidal and H. Moutarde, Eur. Phys. J. A **42**, 71 (2009).
[20] M. Guidal, Phys. Lett. B **689**, 156 (2010).
[21] M. Guidal, Phys. Lett. B **693**, 17 (2010).
[22] M. Boër and M. Guidal, J. Phys. G **42** (2015) no.3, 034023 doi:10.1088/0954-3899/42/3/034023

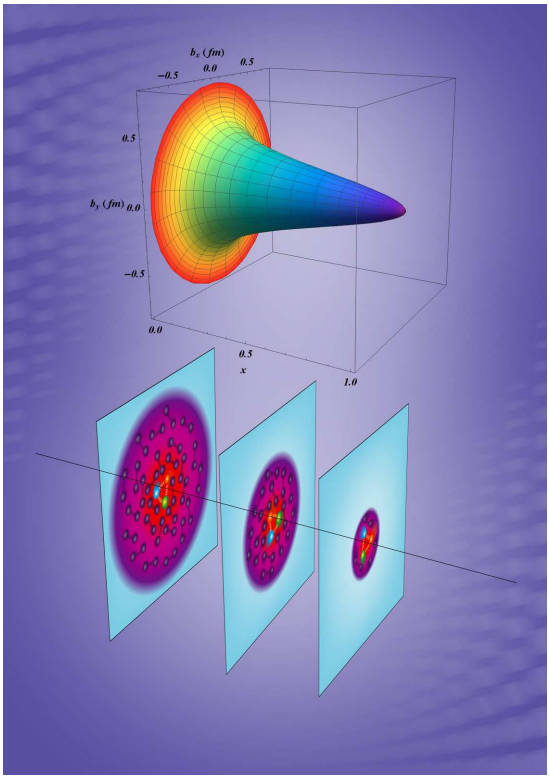

Fig. 4: Top panel: three-dimensional representation of the quark-momentum dependence of the proton's transverse charge radius. Bottom panel: artistic illustration of the corresponding rising quark density and transverse extent as a function of their longitudinal momentum.

[23] K. Kumericki and D. Müller, Int. J. Mod. Phys. Conf. Ser. **40** (2016) 1660047.
[24] R. Dupré, M. Guidal and M. Vanderhaeghen, Phys. Rev. D **95** no.1, 011501 (2017).
[25] R. Dupré, M. Guidal, S. Niccolai and M. Vanderhaeghen, arXiv:1704.07330 [hep-ph].
[26] M. Defurne *et al.* [Jefferson Lab Hall A Collaboration], Phys. Rev. C **92** 5, 055202 (2015).
[27] H. S. Jo *et al.* [CLAS Collaboration], Phys. Rev. Lett. **115**, 212003 (2015).
[28] E. Seder *et al.* [CLAS Collaboration], Phys. Rev. Lett. **114** 3, 032001 (2015) [Phys. Rev. Lett. **114** 8, 089901 (2015)].
[29] S. Pisano *et al.* [CLAS Collaboration], Phys. Rev. D **91** 5, 052014 (2015).